PCCP

Accepted Manuscript

This is an *Accepted Manuscript*, which has been through the Royal Society of Chemistry peer review process and has been accepted for publication.

Accepted Manuscripts are published online shortly after acceptance, before technical editing, formatting and proof reading. Using this free service, authors can make their results available to the community, in citable form, before we publish the edited article. We will replace this *Accepted Manuscript* with the edited and formatted *Advance Article* as soon as it is available.

You can find more information about *Accepted Manuscripts* in the **Information for Authors**.

Please note that technical editing may introduce minor changes to the text and/or graphics, which may alter content. The journal's standard **Terms & Conditions** and the **Ethical guidelines** still apply. In no event shall the Royal Society of Chemistry be held responsible for any errors or omissions in this *Accepted Manuscript* or any consequences arising from the use of any information it contains.

www.rsc.org/pccp

ARTICLE TYPE

QCM study of ORR-OER and in-situ study of a redox mediator in DMSO for Li-O$_2$ batteries

Stijn Schaltin,[a] **Gijs Vanhoutte,**[a] **Minxian Wu,**[a] **Fanny Bardé**[*b] **and Jan Fransaer**[*a]

The oxygen reduction reaction and oxygen evolution reaction (ORR-OER) in DMSO were investigated by cyclic voltammetry and potentiostatic methods. Quartz crystal microbalance (QCM) was used to detect which products are formed during reduction and to evaluate the reversibility of the reactions. The studied parameters include the scan rate and the applied cathodic potential. We confirm by QCM that LiO$_2$ is soluble: this conclusion comes from the time delay we observed between the deposition of the expected mass (based on Faraday's law) and the measured mass. Ambiguity in reported literature values for the slope of the deposited mass per electron $\frac{M}{z}$ is due to the negligence in considering this time delay. The average $\frac{M}{z}$ value versus cathodic charge indicates that soluble LiO$_2$ is the first product of the ORR which reacts further to form Li$_2$O$_2$, either via a disproportionation reaction or via further electrochemical reduction of LiO$_2$. For strong negative potentials, thus large depths of discharge, Li$_2$O is the main discharge product. The reaction pathways hence strongly depend on the experimental conditions applied; especially the reduction potential. The redox mediator tetrathiafulvalene (TTF) was investigated and its influence on reversibility confirmed for cycling at moderate depth of discharge, where Li$_2$O$_2$ is the main discharge product.

1 Introduction

Metal/air batteries are unique in the sense that the active cathode material, which is oxygen gas, is not stored in the battery. It diffuses into the battery during the discharge process from the outside environment and is consecutively reduced at the surface of the air electrode. During the charge process, oxygen gas is formed, which is given back off to the outside atmosphere. In non-aqueous solutions, the dissolved oxygen gas is reduced to superoxide O$_2^-$, which can react further to metal peroxides or metal oxides with metal ions which are present in the solution. Such metal-air batteries have a much higher theoretical specific energy than most other primary and rechargeable batteries.[1] This is especially true for Li-air batteries due to the high specific energy of lithium metal. Li-oxygen batteries were first introduced by Abraham and Jiang[2] who used a conductive organic polymer as the electrolyte and since then, many other solvents were investigated. Examples are propylene carbonate, ethylene carbonate, 1,2-dimethoxyethane (DME), diethylene glycol diethyl ether (diglyme), tetraethylene glycol dimethyl ether (tetraglyme), sulfone-based electrolytes, ionic liquids and acetonitrile.[3–14] Not all of these solvents can be used in lithium-oxygen batteries because some of them are unstable in the presence of the superoxide radical, as is the case for organic carbonates and sulfones.[5–7,13,15] Extensive analyses have been dedicated to dimethylsulfoxide (DMSO) which proves to be one of the most stable solvents, together with DME, acetonitrile and some ionic liquids.[15,16] However, recent papers questioned the stability of DMSO in long term experimental conditions[17,18] or in battery configuration utilizing low electrolyte volume combined with high surface area carbon electrodes.[19] Kwabi *et al.* showed that DMSO can react with Li$_2$O$_2$ if given enough time (up to several weeks).[17] The fact that this reactivity was not mentioned before is attributed to the short charge/discharge time typically used in lab-scale experiments. ORR/OER were thoroughly studied in DMSO.[18–25] However, the products that are formed after the reduction of oxygen to superoxide have only scarcely been analyzed by quartz crystal microbalance techniques (QCM).[19,26] QCM is an excellent technique to measure the amount of mass deposited on the working electrode. In this work we will use the QCM to compare the experimental mass with possible theoretical masses, based on the charge passed through the electrodes and Faraday's law, to determine the composition of the deposited compound. Our study will be performed in Li-containing DMSO with and without tetrathiafulvalene (TTF). The use of TTF as an electron-hole transfer agent to aid the oxidation of Li$_2$O$_2$ has already been reported by Chen *et al.*[27] and its efficacy confirmed by mass spectroscopy. Here we will investigate its activity using QCM so that its effect can be determined from a mass point-of-view.

[a] *KU Leuven - Kasteelpark Arenberg 44 - box 2450, B-3001 Heverlee, Belgium. jan.fransaer@mtm.kuleuven.be*
[b] *Toyota Motor Europe, Advanced Technology 1, Research and Development 3 - Technical Center, Hoge Wei 33B, B-1930 Zaventem, Belgium. Fanny.Barde@toyota-europe.com*

2 Experimental

Tetrabutylammonium perchlorate (TBAP), DMSO ($<$55 ppm H_2O) and lithium bis(trifluoromethylsulfonyl)imide (LiTf$_2$N) (1 M solution in DMSO ($<$50 ppm H_2O)) were purchased from BASF. The water content was analyzed by Karl Fischer titration and was found to be below 55 ppm. Tetrathiafulvalene (TTF, 97%) was bought from Sigma-Aldrich. When used, the concentration of TTF was about 5 mM. The solutions were transferred into a home-made cell (figure 1) inside an argon-filled glove box. The sealed cell was then taken out of the glove box and connected to an oxygen supply after which oxygen gas ($H_2O<0.5$ ppm, $CO_2 <0.1$ ppm) was bubbled through the solution until the electrolyte was saturated with molecular oxygen.

All potential values in this paper are relative to Li^+/Li. Nevertheless, since lithium is incompatible with DMSO, we used a silver wire as a pseudo reference electrode. The measured potentials were then calibrated and expressed relative to Li^+/Li. A platinum coil was used as counter electrode. As working electrode, gold covered QCM-crystals were used with an electrochemically active surface area of 1.37 cm^2. Experiments were executed at room temperature with the Quartz Crystal Microbalance (Maxtex RQCM) connected to a Potentiostat/Galvanostat EG&G 273. A schematic of the setup (with the crystal in a horizontal position) is shown in figure 1. Interactions between the solvent and the Kalrez O-rings could lead to a drift in the QCM-signal, even in the absence of electrochemical reactions. If the drift was linear, the Δf signals were corrected for this drift. In case of a non-linear drift, the cell was disassembled and the experiment repeated.

3 Results and discussion

3.1 Potential-scan experiments

Cyclic voltammetric experiments were conducted on oxygen-saturated DMSO-solutions with or without Li^+ salt. Gold was chosen as the material for the working electrode in order to avoid any possible interactions of carbon with the electrolyte. Indeed, in the literature, most experiments are performed with glassy carbon electrodes, and while it has been reported that glassy carbon and gold give nearly identical responses, [21] there are also studies highlighting that carbon electrodes promote electrolyte decomposition in Li-O$_2$ cells forming lithium carbonates and carboxylates. [28]

In the absence of a Li^+ salt, TBAP was used as the supporting electrolyte. Tetraalkylammonium perchlorate salts such as TBAP give identical results in a range of solvents for the study of the electrochemistry of molecular oxygen [11]. Figure 2 shows the cyclic voltammograms, measured with a constant anodic vertex potential of +0.5 V and cathodic vertices of 2.6,

(a)

(b)
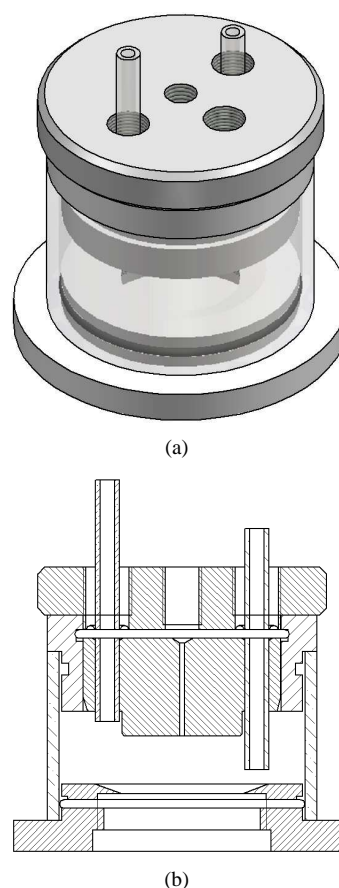
Fig. 1 Schematic of the setup: the top-lid has 4 feed-throughs (O$_2$ in, O$_2$ out, reference electrode, counter electrode) sealed with O-rings. The cell contains $7-8$ ml of electrolyte. This whole setup can be screwed on a commercial Maxtex RQCM-crystal holder.

2.4, 2.3 and 2.1 V, for the reaction

$$O_2 + e^- \rightleftharpoons O_2^- \qquad (1)$$

which can be written too as [20]

$$TBA^+ + O_2 + e^- \rightleftharpoons TBAO_2 \qquad (2)$$

The reduction of molecular oxygen to the superoxide ion starts at 2.7 V. Upon reversing the scan direction, an anodic peak develops indicating that the oxidation of the superoxide anion is reversible, in correspondence with literature data for this reaction in DMSO. [20]

To study the electrochemistry of the ORR/OER in Li^+-containing solutions, lithium ions were added as LiTf$_2$N. This salt was chosen based on the conclusions of Xu *et al.* who claim that this salt is the best for ambient operations of Li/air batteries (in propylene carbonate/ethylene carbonate mixtures). [3,4] Furthermore, Chen *et al.* reported that changing
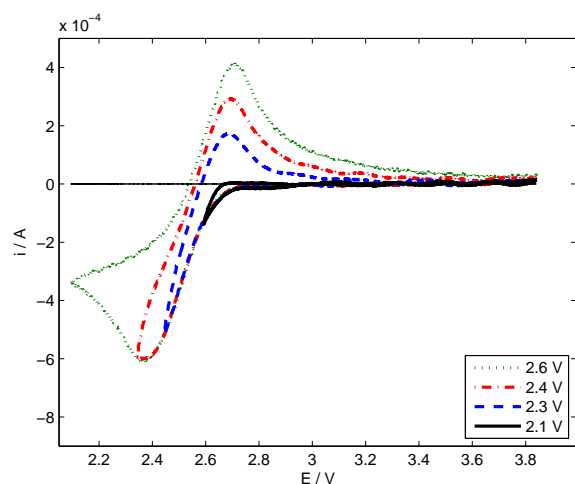
Fig. 2 Cyclic voltammogram (solid line) of an oxygen saturated DMSO solution containing 0.1 M of TBAP. The scan rate was 50 mV s^{-1} and the different line styles indicate different cathodic vertex potentials.

Fig. 3 Cyclic voltammograms of an oxygen saturated DMSO solution containing 0.1 M of Li$^+$. The scan rate was 50 mV s^{-1} and the different line styles indicate different cathodic vertex potentials.

the lithium salt (LiClO$_4$, LiPF$_6$ or LiTf$_2$N) did not lead to different charging cycles,[27] a result confirmed by Peng *et al.*[29] The voltammograms of 0.1 M Li$^+$ in oxygenated DMSO are quite different from those without Li$^+$ (figure 3). If the cathodic vertex potential is limited to the range 2.6 V − 2.4 V, a single peak is observed at 2.8 V in the corresponding anodic scan. For intermediate cathodic vertex potentials (2.3 V), the anodic peak at 2.8 V decreases slightly and a peak appears at 3.2 V. For more negative cathodic vertex potentials, only an anodic peak at 3.2 V remains. These observations correspond with the measurements reported by Abraham *et al.*[20,21] and are attributed to the following reactions:

$$Li^+ + O_2 + e^- \rightarrow LiO_{2(sol)} \tag{3}$$

$$Li^+ + O_2 + e^- \rightarrow LiO_2 \downarrow \tag{4}$$

$$2LiO_2 \rightarrow Li_2O_2 \downarrow + O_2 \tag{5}$$

$$LiO_2 + Li^+ + e^- \rightarrow Li_2O_2 \downarrow \tag{6}$$

$$Li_2O_2 + 2Li^+ + 2e^- \rightarrow 2Li_2O \downarrow \tag{7}$$
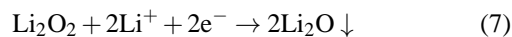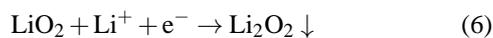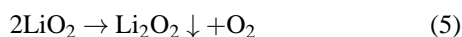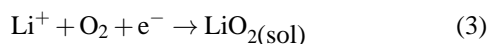
Note that Abraham *et al.* did not discriminate reactions (3) and (4) as we do here depending whether LiO$_2$ is soluble or a solid. This point will be discuss further later in this paper.

The cathodic reaction is due to the formation of the superoxide LiO$_2$ (reaction (3) which itself is the sum of reaction (1) and O$_2^-$ + Li$^+$ → LiO$_2$)), which disproportionates to Li$_2$O$_2$ via reaction (5) or is reduced further according to reaction (6). Li$_2$O$_2$ itself might later be reduced to Li$_2$O (reaction (7)) but

if reactions (3), (6) and (7) happen consecutively and fast, they can be written as a single reaction (8).

$$4Li^+ + O_2 + 4e^- \rightarrow 2Li_2O \tag{8}$$

Although the presence of Li$_2$O at the end of discharge and especially its oxidation on charge remains a point of debate,[20] recent in situ X-ray photoelectron spectroscopy (XPS) studies on Li-oxygen electrochemistry clearly show evidence of the formation and oxidation of Li$_2$O when solid-state electrolytes are used.[30,31] The anodic peaks at 2.8 V and -3.2 V are then assigned to the oxidation of LiO$_2$ and Li$_2$O$_2$, respectively. During reoxidation, Li$_2$O$_2$ follows the direct oxidation path to O$_2$ without the formation of LiO$_2$ (reaction (9))[11,12]

$$Li_2O_2 \rightarrow 2Li^+ + O_2 + 2e^- \tag{9}$$
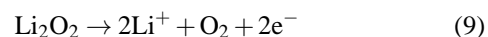
In cyclic voltammetry experiments, the oxidation peak of LiO$_2$ appears because of the relative short time scales considered, but in real battery applications we estimate that all LiO$_2$ will have disproportionated according to reaction (5).[11,12]

QCM was employed to study the deposition products and mechanism of the oxygen reduction reaction in Li$^+$-containing DMSO, with and without the presence of the redox mediator TTF. As a reference situation, figure 4 shows both the cyclic voltammetry (solid line) and the QCM signal (dotted line) of an oxygen saturated DMSO solution containing 0.1 M TBAP and 5 mM TTF, but in the absence of Li$^+$. As expected, the figure confirms that the reduction of O$_2$ to TBAO$_2$ or the oxidation of the redox mediator TTF to TTF$^+$ and TTF^{2+} and their backreactions does not result in a change of Δf (figure 4, dotted line) demonstrating that none of these
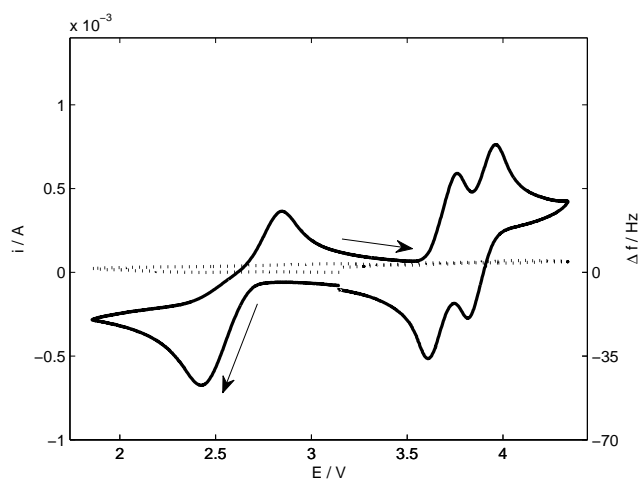
Fig. 4 Cyclic voltammogram (solid line, left axis) of an oxygen saturated DMSO solution containing 0.1 M of TBAP and TTF with QCM analysis (dotted line, right axis). The scan rate was 50 mV s^{-1}.

reactions leads to the formation of a solid product. It also confirms that DMSO is stable towards O_2^- during the time, and under the conditions, of the experiment.

Figure 5(a) shows the cyclic voltammogram (solid line) of an oxygen saturated DMSO solution containing 0.1 M of Li^+ with QCM analysis (dotted line) in the absence of TTF. The dashed line represents the theoretical curve Δf_t under the assumption that Li_2O_2 is the end product of all consumed charge. This is accomplished by combining the Sauerbrey equation and Faraday's law of electrochemistry

$$m = -C\Delta f \tag{10}$$

$$m = \frac{MQ}{z\mathrm{F}} \tag{11}$$

where m is the mass deposited on the quartz crystal, $Q = \int_0^t i(\tau)\, d\tau$, M is the molar mass of the deposited compound, z is the number of electrons in the electrochemical reaction, F is the Faraday constant and C is the proportionality constant in Sauerbrey equation. This constant C was experimentally determined for our QCM set-up by silver deposition from DMSO.[32,33] Equation (10) states that an increase in deposited mass leads to a negative shift in the resonance frequency f. At first sight it appears that there is discrepancy between the experimental Δf and theoretical Δf_t. It is however important to mention that in the Li-O_2 system the variation of Δf (i.c. deposition) does not happen simultaneously with i as is the case for metal deposition. It was reported that the reduction of oxygen leads to soluble superoxide.[21,25] Therefore we expect a time delay between the moment these species are formed, and disproportionate by reaction (5), and the moment they deposit on
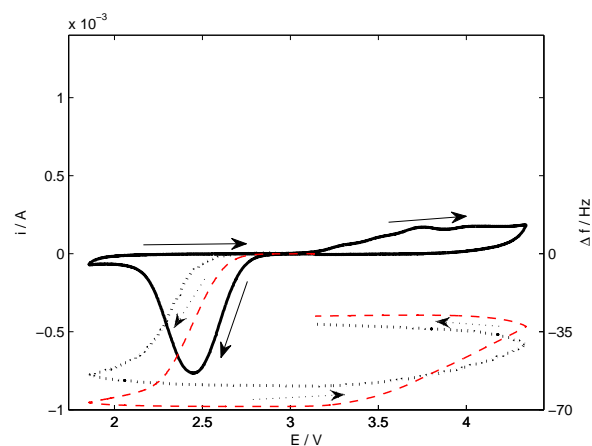
(a) 50 mV s^{-1}, no TTF
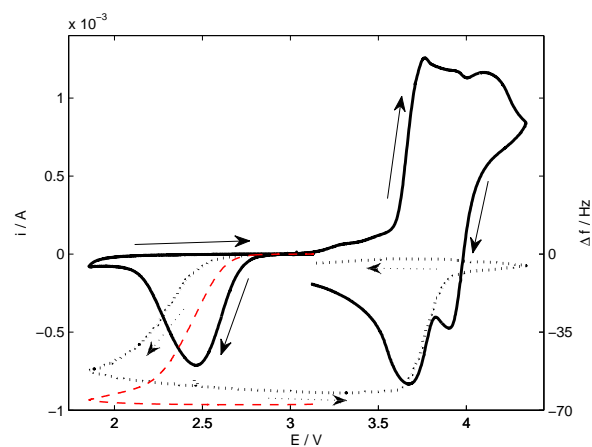
(b) 50 mV s^{-1}, 5 mM TTF
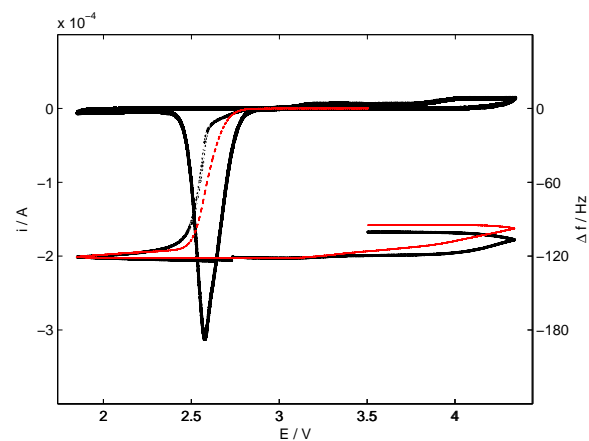
(c) 5 mV s^{-1}, no TTF

Fig. 5 Cyclic voltammogram (solid line) of an oxygen saturated DMSO solution containing 0.1 M of Li^+ with QCM analysis (dotted line). The red dashed line represents the expected Δf_t curve for Li_2O_2.

the electrode. That time delay is the reason why the experimental Δf lags the theoretical Δf_t which assumes an instantaneous correlation between the charge Q (and hence the current $i(t)$) and the deposited mass m. By the time the measured current reaches zero, Δf is still lower than Δf_t. This can be accounted for by the solubility of the superoxide species: Δf_t assumes that all the reaction products end up on the electrode but due to the solubility of LiO_2 in DMSO, part of it diffuses into the bulk and is lost. The anodic part of the voltammogram, together with the fact that Δf does not reach zero, shows that reaction (9) is incomplete so that at the end of the anodic cycle some Li_2O_2, that formed during the cathodic cycle, is still present on the electrode. This means that the ORR/OER is not fully reversible. A similar analysis was performed for a solution with 5 mM of TTF and is shown in figure 5(b). Note that the curve for Δf_t is limited to the cathodic part since it cannot be calculated in the anodic part due to the fact that the anodic current consist of the oxidation of both TTF and Li_2O_2. The cathodic half of the experiment is identical to the experiment without TTF, since TTF does not influence the ORR. In the anodic half it is clear that the experimental Δf starts to fall back to zero as soon as the formation of TTF^+ (and TTF^{2+}) starts, proving that the oxidized TTF quickly removes the deposited Li_2O_2 from the electrode. The most likely pathway for this reaction is an extension from reaction (9):

$$Li_2O_2 + 2TTF^+ \rightarrow 2Li^+ + O_2 + 2TTF \qquad (12)$$

$$Li_2O_2 + TTF^{2+} \rightarrow 2Li^+ + O_2 + TTF \qquad (13)$$
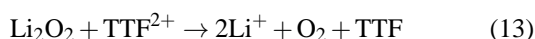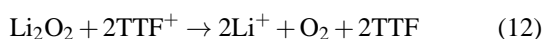
The effective removal of the products of the ORR proves that a redox mediator can be activated in-situ and acts immediately to decompose Li_2O_2. The peaks for the oxidation of TTF look distorted when figure 5(b) is compared with figure 4. In a solution without Li^+, TTF^+ can be oxidized further to TTF^{2+} at potentials above +0.5 V which leads to a new oxidation peak. When discharge products are deposited on the electrode, much less TTF^+ is available for further oxidation because it reacts with the discharge products and is reduced chemically back to TTF. This leads to the observation that the second oxidation peak for TTF is smaller than the first. Finally, an experiment was conducted at 5 mV s^{-1} in the absence of TTF (figure 5(c)). The slower scan rate has several effects. The measured currents are smaller and the Coulombic efficiency drops because of the very low anodic current. Nevertheless, Li_2O_2 is still the best match for the experimentally determined mass.

Figure 6 shows the mass m vs. charge Q plots based on the voltammograms of figure 5. Q is the amount of charge obtained by integrating the current and the mass m is found from Δf by using eq. (10). The data are limited to the cathodic half-cycle of the voltammogram (3.1 V $\rightarrow$ 1.8 V $\rightarrow$ 3.1 V) so that the electrochemistry of TTF is not involved. The advantage of plotting the data in an m vs. Q plot is that the slope of this curve is $\frac{M}{zF}$ (see equation (11)) so that it can be used to determine the ratio $\frac{M}{z}$ (ratio of the molar mass of the added load on the electrode to the number of electrons consumed in the reaction).

Table 1 M (in g mol^{-1}), z and $\frac{M}{z}$ (in g mol^{-1}) values, and related end products expected for the (electro)chemical reactions (3)$-$(8)

Reactions	Deposited mass	M	z	$\frac{M}{z}$	End product
(3)	-	0	1	0	$LiO_2{}_{(sol)}$
(4)	Li, 2O	38.9	1	38.9	LiO_2
(3)+(3)+(5)	2Li, 2O	45.9	2	22.9	Li_2O_2
(3)+(6)	Li	45.9	2	22.9	Li_2O_2
(7)	2Li	13.9	2	6.9	$2Li_2O$
(8)	4Li, 2O	59.8	4	14.9	$2Li_2O$

Table 1 shows the M, z, and $\frac{M}{z}$ values, and related products expected for the (electro)chemical reactions (3)$-$(8). Reaction (3) has a $\frac{M}{z}$ ratio of zero because LiO_2 is a soluble species[21,25] (which we confirmed by our own RRDE experiments: see supporting information). The $\frac{M}{z}$ ratio for reaction (5) would be infinite since it is a chemical, not an electrochemical, reaction which can form a deposit without the need of an externally applied current of electrons. Nevertheless, reaction (5) can only take place if LiO_2 is present in the solution. So table 1 mentions reaction (5) only together with reaction (3). The combination of these reactions leads to Li_2O_2 with an average $\frac{M}{z}$ of 22.9 g mol^{-1}. Similarly, reaction (6) cannot happen on its own but only after reaction (3). In case of Li_2O, we add a coefficient of 2 so that all values are referred to one molecule of O_2. For the formation of Li_2O, there are two possible reaction pathways leading to a $\frac{M}{z}$ of 6.9 g mol^{-1} or 14.9 g mol^{-1} depending whether Li_2O_2 is a reactant already present on the electrode (reaction (7)) or that all reactants are soluble (reaction (8)).

A similar analysis of the ORR was already done in literature[26], yet we believe the analysis was incomplete. The solubility of LiO_2 was not taken into account and no interpretation was given for the potential region more negative than the peak potential, although it accounts for almost half the consumed charge. The theoretical $\frac{M}{z}$ value of 38.9 g mol^{-1} can only be achieved if all LiO_2 is deposited and nothing is lost into solution (reaction (4)). This is contradictory to the work of Trahan *et al.* and Johnson *et al.*[21,34] So the fact that superoxide is soluble prohibits the detection of this high value of 38.9 g mol^{-1} and the reaction happening is reaction (3) and not reaction (4).

Indeed, figure 6(a) shows that at the start of the reduction, the slope of the curve corresponds to an $\frac{M}{z}$ of only 4.3 g mol^{-1} in the potential range of 3.1 $-$ 2.5 V but continuously increases to a value of 43.7 g mol^{-1} in the range 2.3 $-$ 1.8 V.

(a) 50 mV s^{-1}, no TTF

(b) 50 mV s^{-1}, 5 mM TTF

(c) 5 mV s^{-1}, no TTF
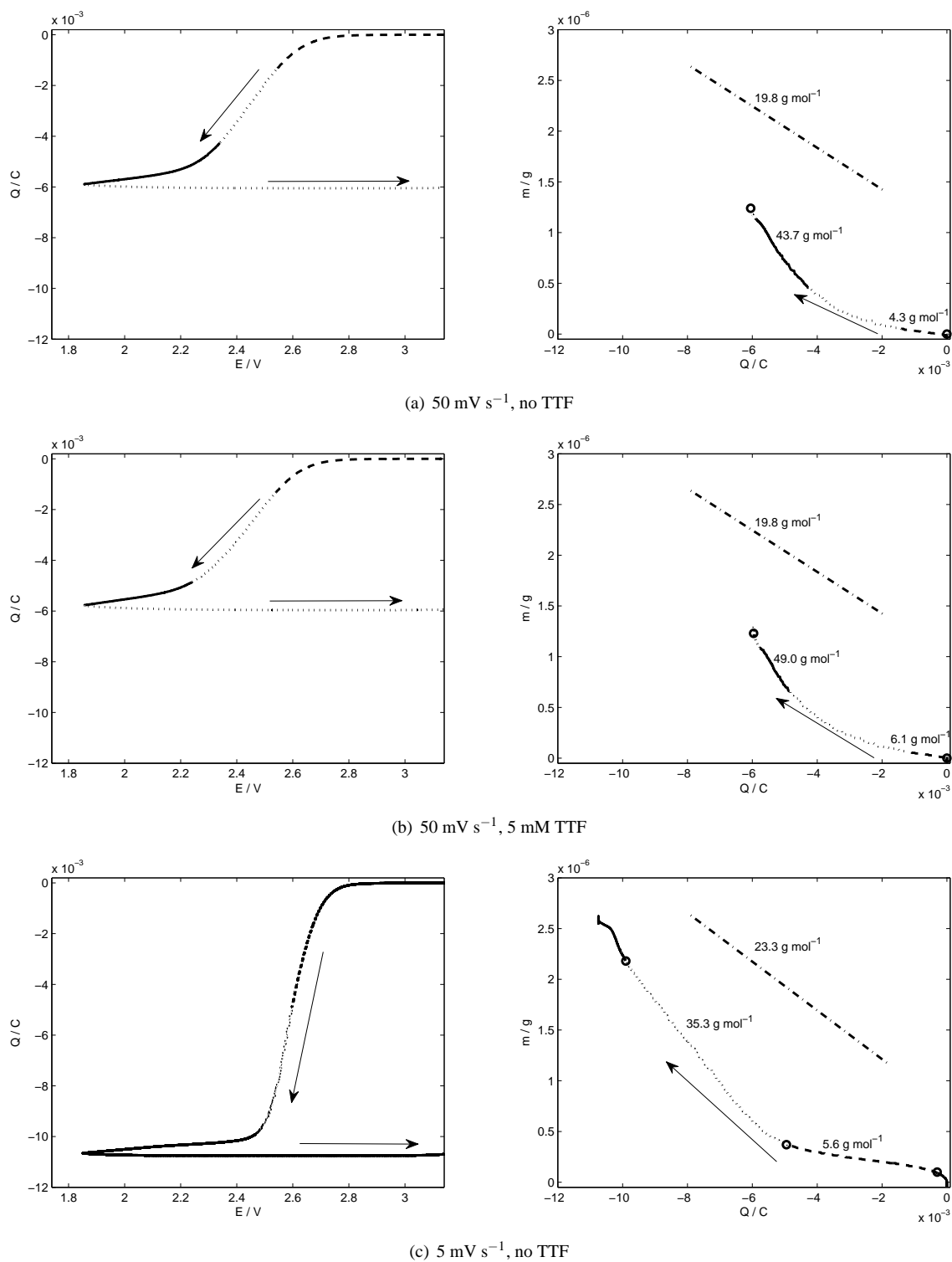
Fig. 6 m vs. Q plots based on the voltammogram of an oxygen saturated DMSO solution containing 0.1 M of Li$^+$ (cfr. figure 5). The plots on the left hand side indicate which Q value corresponds to which E value: the different line styles clarify the different potential regions. The dash-dotted lines indicated the average slopes of 19.8 and 23.3 g mol^{-1}.

At first, one would thus believe that in the beginning of the reduction the deposition is inefficient and that the majority of the current is carried by the reduction of O_2 to O_2^- without the superoxide forming a deposit on the electrode and that at more negative potentials it is mostly LiO_2 that forms since the experimental $\frac{M}{z}$ value of 43.7 g mol^{-1} is the closest to the theoretical value of 38.9 g mol^{-1}. But, as mentioned earlier, LiO_2 is a soluble species so that the electrochemical reaction of its formation has an $\frac{M}{z}$ value of 0 g mol^{-1} (table 1). Furthermore, from figure 5 it is clear that there is a time delay between the theoretical Δf_t and the experimental Δf. A point-by-point analysis of an m vs. Q-plot is hence not correct, because such analysis is based on Faraday's law (equation (11)). This law assumes a simultaneous relationship between the passage of current and the deposition of mass but neglects the possibility of soluble species. As a consequence, we looked at an average value that takes into account the entire reductive half-cycle of the voltammogram. The disadvantage of this approach is the loss of voltage-dependent information, but this information can be found during potential-hold experiments (§3.2). As an advantage, the time delay can be circumvented if the studied timeframe is large enough. The starting point of the voltammogram of figure 5(a) and the end point of its reductive half-cycle correspond to the points with $(Q; M)$ coordinates (0 C; 0 g) and (-6·10^{-3} C; 12.4·10^{-7} g) in figure 6(a), and the average slope between these points gives an $\frac{M}{z}$ of 19.8 g mol^{-1}. A similar analysis of the data in figure 6(b) gives the same result because the data are limited to the potential region where TTF is not yet oxidized. This measured $\frac{M}{z}$ value is close to the theoretical $\frac{M}{z}$ value of 22.9 g mol^{-1} related to the formation of Li_2O_2 (table 1). Li_2O_2 is thus the product detected by QCM. The fact that the measured $\frac{M}{z}$ is lower than expected can be due to the fact that O_2^- also binds with impurities or the solvent,[17] that some Li_2O_2 has already been reduced further to Li_2O by reaction (7) or by LiO_2 that is lost to the bulk of the solution. Since the $\frac{M}{z}$ value for Li_2O is only 14.9 g mol^{-1} and the loss of LiO_2 corresponds to an $\frac{M}{z}$ value of 0 g mol^{-1} (table 1), this decreases the measured average $\frac{M}{z}$. An equivalent analysis of the data from figure 6(c) for the voltammogram at 5 mV s^{-1} gives an average $\frac{M}{z}$ of 23.3 g mol^{-1}. Again: close to the theoretical value for Li_2O_2.

Figures 7(a) and (b) show the superposition of ten consecutive cycles performed within the $1.8 - 4.3$ V window for an oxygen saturated 0.1 M Li$^+$-DMSO electrolyte not containing TTF at 5 mV s^{-1} and 50 mV s^{-1}, respectively. After a few cycles, the system gets in a *steady-state* where the different cycles overlap. Table 2 shows the cathodic and anodic charges Q_c and Q_a, and the Coulombic efficiencies η_C for the voltammograms of figure 7 (cycles 1−5, 10). Several differences are noticed when the scan rate is changed: Q_c is, on average, almost twice as high at a scan rate of 5 mV s^{-1}. This

Table 2 Cathodic and anodic charges (Q_c and Q_a, in mC) and Coulombic efficiencies ($\eta_C = \frac{Q_a}{Q_c}$, in %) for the voltammograms shown in figures 7.

Cycle ♯	5 mV s^{-1}			50 mV s^{-1}		
	Q_c	Q_a	η_C	Q_c	Q_a	η_C
1	11.3	2.3	21	5.1	2.9	57
2	7.6	2.0	26	4.9	3.2	65
3	7.1	2.3	32	4.7	3.2	68
4	8.4	2.7	32	4.6	3.3	72
5	8.4	2.6	31	4.3	3.0	70
10	8.3	2.7	33	4.3	3.2	74

is not surprising considering that at low scan rates more time is spent in the potential region where oxygen reduction occurs. On the other hand, Q_a is smaller at low scan rates. As a result, the Coulombic efficiency is much smaller at 5 mV s^{-1} than at 50 mV s^{-1} (see table 2). With this information we can explain why there is a better correspondence between the Δf and Δf_t at 5 mV s^{-1} than at 50 mV s^{-1}. At both scan rates, LiO_2 is the discharge product that forms first and it is formed in larger amounts (larger Q_c) at 5 mV s^{-1} since the time during which the potential is in the oxygen reduction range is longer. As a consequence, the solution in the vicinity of the electrode is depleted in O_2 while it is enriched in LiO_2 and the combination of these two factors shifts the chemical equilibrium of reaction (5) to the right. Since the chemical formation of Li_2O_2 is favored at 5 mV s^{-1} and less LiO_2 is lost in solution, a better correspondence is found between the experimental Δf and theoretical Δf_t. The different pathway of how Li_2O_2 is formed can also explain the difference in oxidation behavior during the positive scans. Xia *et al.* found that the chemical formation of Li_2O_2 leads to a toroidal structure while the electrochemical pathway gives a film morphology.[35] The latter structure has a lower overpotential for oxidation so that it is more reversible and results in higher Coulombic efficiencies (table 2). Similar findings were reported by Adams *et al.*[36] Those studies were not in DMSO, but the authors claim that the implications of their results can be carried over to other systems.

3.2 Potential-hold experiments

We also studied the reversibility of the ORR/OER. Cyclic voltammetry is not the right technique to study reversibility in this system because the continuous scan of the potential causes the driving force for electrochemical reactions to constantly change. Together with the time delay, this severely complicates the study. In literature, reversibility is often studied by galvanostatic cycling: an anodic and cathodic current are consecutively applied. In this study, we controlled the potential instead of the current to make sure that the potential stayed within the electrochemical stability window of DMSO.

(a) 5 mV s^{-1}
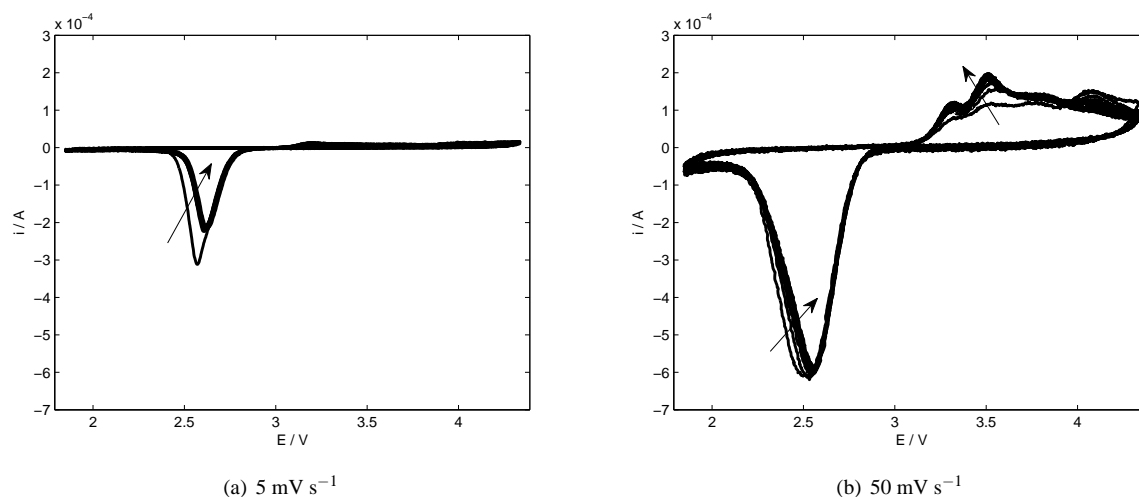
(b) 50 mV s^{-1}

Fig. 7 Cyclic voltammograms of an oxygen saturated DMSO solution containing 0.1 M of Li$^+$ for ten cycles at 5 and 50 mV s^{-1}. The arrows indicate the change of the voltammograms with increasing number of cycles.

The anodic potential was fixed to 4.3 V, a value that corresponds to the anodic vertex of the voltammograms in figure 5, while the cathodic potential was set to 2.6 V, 2.4 V or 1.8 V, values which correspond to the maximum, the middle, and the end of the cathodic peak corresponding to ORR (figure 7(a)), respectively. The results are plotted in figures 8−11. The cathodic pulse was held for 10 s, the anodic pulse for 60 s. This asymmetry was selected to allow the products formed during reduction to have enough time to reoxidize. The potential was pulsed from open circuit to either 2.6, 2.4 or 1.8 V and then to 4.3 V (the E vs. t functions are added to the figures: *vide infra*). In total, ten cathodic pulses were applied. Figure 8 shows the results for a cathodic pulse to 2.6 V. The 10 s cathodic polarization is not long enough to bring the current back to zero, but the 60 s anodic polarization is. From an electrochemical point of view, the process is not completely reversible: there is a net excess of cathodic charge. From a QCM viewpoint the process is reversible but for the first cycle the experimental mass is too small for Li$_2$O$_2$ to account for it (also if LiO$_2$ is considered). Also during the first cycle, the measured $\frac{M}{z}$ ratio is 7.5 g mol^{-1} (see figure 8(b)). This is further proof that not all reduced species deposit on the electrode. In later pulses, the $\frac{M}{z}$ value stabilizes at 27.7−27.9 g mol^{-1} (table 3). These results indicate that only LiO$_2$ is formed electrochemically by reaction (3). There is simply not enough driving force for reactions (6)-(7) to happen because the potential is not negative enough. Part of the LiO$_2$ is lost to the bulk of the solution while the part that disproportionates by reaction (5) in the vicinity of the electrode is detected by the QCM. The LiO$_2$ that is lost in the bulk will of course form Li$_2$O$_2$ by disproportionation too. Cycle after cycle, the formed Li$_2$O$_2$

Table 3 Experimental $\frac{M}{z}$ ratios (in g mol^{-1}) during the cycle experiments shown in figures 8 and 9.

Cycle ♯	cathodic potential	
	2.6 V	2.4 V
1	7.5	22.1
2	11.9	9.1
3	18.4	8.0
4	22.8	7.8
5	24.2	7.7
6	27.7	7.2
7	30.2	6.3
8	27.6	6.8
9	29.4	6.6
10	27.9	6.5

will precipitate on the electrode which causes the increase in the measured $\frac{M}{z}$ ratios. Figure 9 is analogous to figure 8 but with a cathodic potential of 2.4 V instead of 2.6 V. For this potential, the 10 s cathodic polarization is long enough for the current to almost fall back to zero. Again there is a net excess of cathodic charge, as previously observed for 2.6 V (figure 8). But in contrast with the previous experiments, the QCM results indicate that from a mass point of view, the process is not fully reversible. The $\frac{M}{z}$ ratios for the consecutive cycles are reported in table 3. In the first cycle, $\frac{M}{z}$ equals 22.1 g mol^{-1}, but quickly drops to a value around 7 g mol^{-1} for later cycles. We believe that a potential of 2.4 V is sufficient to form Li$_2$O$_2$ by reaction (6). Right after applying the cathodic pulse, the first reaction happening is reaction (3) and LiO$_2$ is
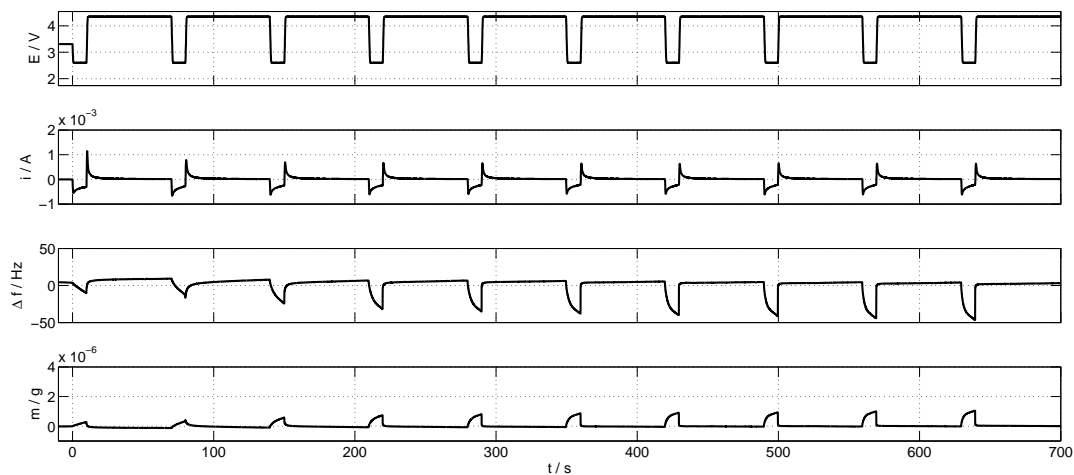
(a) E, i, Δf and m as a function of time
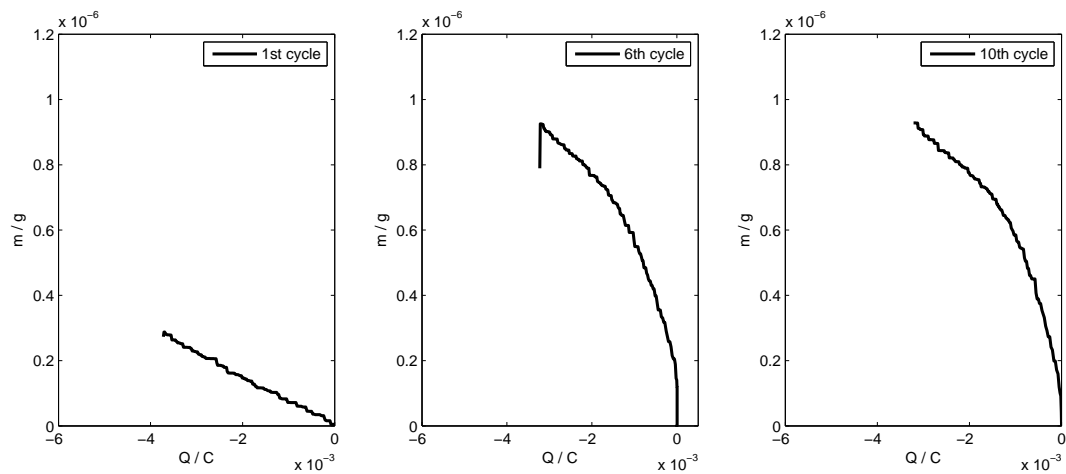
(b) m vs. Q plots for the cathodic part of cycles 1, 6 and 10 of figure (a)

Fig. 8 Potential cycling between 2.6 V (pulse of 10 s) and 4.3 V (pulse of 60 s) on gold of O_2 and 0.1 M of Li^+.
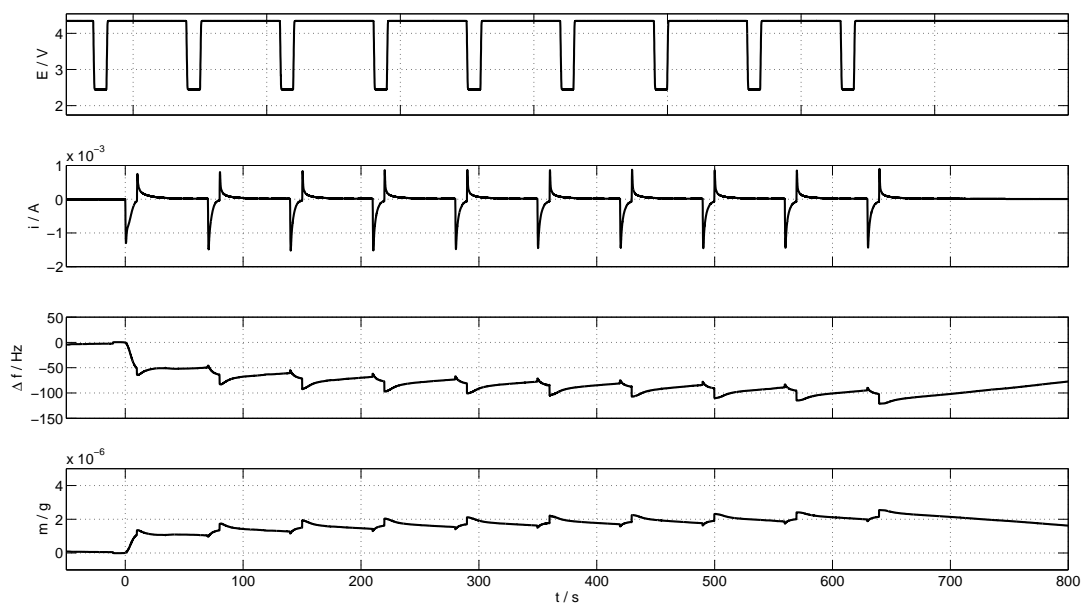
(a) E, i, Δf and m as a function of time
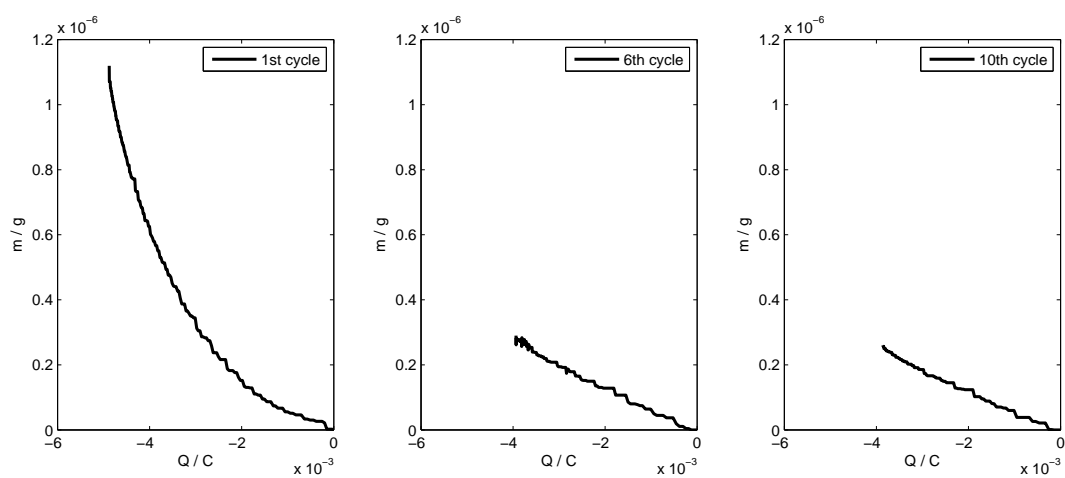
(b) m vs. Q plots for the cathodic part of cycles 1, 6 and 10 of figure (a)

Fig. 9 Potential cycling between 2.4 V (pulse of 10 s) and 4.3 V (pulse of 60 s) of O_2 and 0.1 M of Li^+ on gold.

immediately reduced further to Li_2O_2 by reaction (6). This means that Li_2O_2 is now formed preferably electrochemically instead of chemically by disproportionation. Furthermore, the more negative potential gives rise to a more cathodic current. It has been reported that a larger current changes the structure of deposited Li_2O_2 from toroids to a film morphology.[36] Moreover, higher overpotentials will lead to a higher driving force for nucleation and hence to higher nucleation density and hence denser films. Assuming our deposits are indeed films, the mass we measure by QCM in the first pulse of figure 9 corresponds to a thickness of 3.4 nm. Viswanathan *et al.* found that Li-O$_2$ batteries show a cell death when the thickness of Li_2O_2 is in the range $5-10$ nm because the peroxide film becomes increasingly electrically insulating as it grows, and is no longer capable of supporting electrochemistry at the Li_2O_2-electrolyte interface.[37] A thickness of 3.4 nm still permits to reduce O_2 but the *iR*-drop must thus be sufficiently high so that reaction (6) can no longer be supported and only reaction (3) remains.

Cycling experiments were also conducted in the presence of TTF to see whether it improves the reversibility during potential pulsing. Figure 10(a) is the analogue of figure 9 but with 5 mM of TTF added to the electrolyte. The experiments show that the addition of TTF has a strong effect: it allows to remove all deposits from the electrode so that the process becomes 100% reversible from a mass point of view. Since the anodic polarization is applied for 60 s, an excess of activated TTF is present. It appears that this excess of TTF reoxidizes LiO_2 and/or Li_2O_2 before it can reach the electrode because for later cycles, the deposited mass keeps decreasing. When the amount of activated TTF is reduced by shortening the anodic polarization time to 10 s instead of 60 s (figure 10(b)), the decrease in mass peak height is less for later cycles. Ideally, the anodic polarization is thus halted when the electrode is completely freed from all lithium-oxygen compounds.

The activity of TTF was tested in more extreme conditions by using a cathodic potential of 1.8 V instead of 2.4 V, which corresponds to a deeper depth of discharge. The result (figure 11) shows that in this case, TTF improves the reversibility. Since the mass changes are comparable for all 10 cycles, it seems there is now a better balance between the total deposited mass and the amount of activated TTF. The $\frac{M}{z}$ ratio of the first cathodic pulse in figure 11 is 14.8 g mol^{-1}, very close to the theoretical value of 14.9 g mol^{-1} for the deposition of Li_2O by reaction (8) (table 1). The formation of Li_2O was earlier only noticed in solid-state electrolytes.[30,31] The QCM-data in figure 11 show that TTF can reoxidize Li_2O only partially: over the course of 10 cycles the mass on the electrode is increasing.

4 Conclusions

Our QCM experiments have demonstrated that at moderate depth of discharge the mass reversibility is strongly improved by TTF that act as an electron-hole transfer agent. QCM indicates that the main discharge product of the Li-O$_2$ system in DMSO is Li_2O_2 while for deeper discharge, Li_2O is found which can only be partially decomposed by TTF. Our results give quantitative information on the reversibility from the point of view of deposited mass even though the analysis is complicated by the fact that the superoxide is soluble in DMSO and the possibility to form multiple lithium-oxygen compounds. We found that by changing the scan rate ((dis)charge rate), the equilibrium of the disproportionation reaction is shifted which leads to a change in the deposition mechanism of Li_2O_2. At high scan rates or more negative cathodic voltages (<2.4 V), the electrochemical path seems preferred while the chemical mechanism is more likely to happen at low rates or more anodic voltages (2.6 V). In order to obtain 100% reversibility (in mass) a moderate potential of only 2.6 V has to be applied but this limits the capacity of the Li-O$_2$ system. For potentials of 2.4 V or lower, the reactions become partially irreversible. Further work is ongoing to study the influence of lithium ion concentration on Coulombic reversibility and on reaction pathways.

5 Acknowledgement

References

1 *Handbook of batteries*, ed. D. Linden and T. Reddy, McGraw-Hill, New York, 3rd edn, 2001.

2 K. M. Abraham and Z. Jiang, *J. Electrochem. Soc.*, 1996, **143**, 1–5.

3 W. Xu, J. Xiao, D. Wang, J. Zhang and J.-G. Zhang, *J. Electrochem. Soc.*, 2010, **157**, A219–A224.

4 W. Xu, J. Xiao, J. Zhang, D. Wang and J.-G. Zhang, *J. Electrochem. Soc.*, 2009, **156**, A773–A779.

5 S. A. Freunberger, Y. Chen, N. E. Drewett, L. J. Hardwick, F. Bardé and P. G. Bruce, *Angew. Chem. Int. Ed.*, 2011, **50**, 8609–8613.

6 S. A. Freunberger, Y. Chen, Z. Peng, J. M. Griffin, L. J. Hardwick, F. Bardé, P. Novák and P. G. Bruce, *J. Am. Chem. Soc.*, 2011, **133**, 8040–8047.

7 F. Mizuno, S. Nakanishi, A. Shirasawa, K. Takechi, T. Shiga, H. Nishikoori and H. Iba, *Electrochemistry*, 2011, **79**, 876–881.

8 C. O. Laoire, S. Mukerjee, E. J. Plichta, M. A. Hendrickson and K. M. Abraham, *J. Electrochem. Soc.*, 2011, **158**, A302–A308.

9 J. Herranz, A. Garsuch and H. A. Gasteiger, *J. Phys. Chem. C*, 2012, **116**, 19084–19094.

10 B. M. Gallant, D. G. Kwabi, R. R. Mitchell, J. Zhou, C. V. Thompson and Y. Shao-Horn, *Energy Environ. Sci.*, 2013, **6**, 2518–2528.
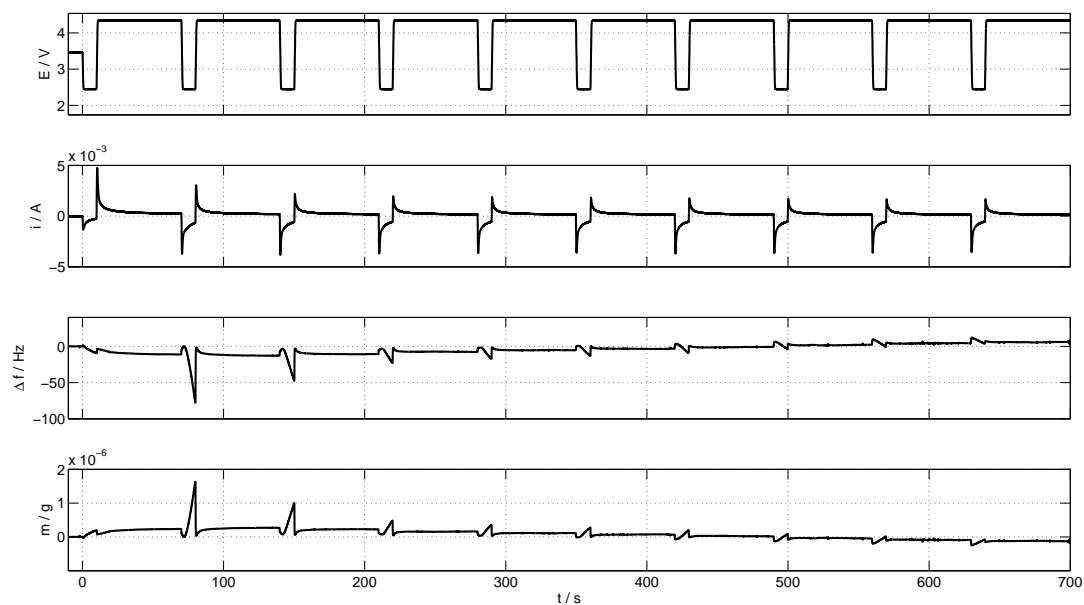
(a) 60 s anodic polarization
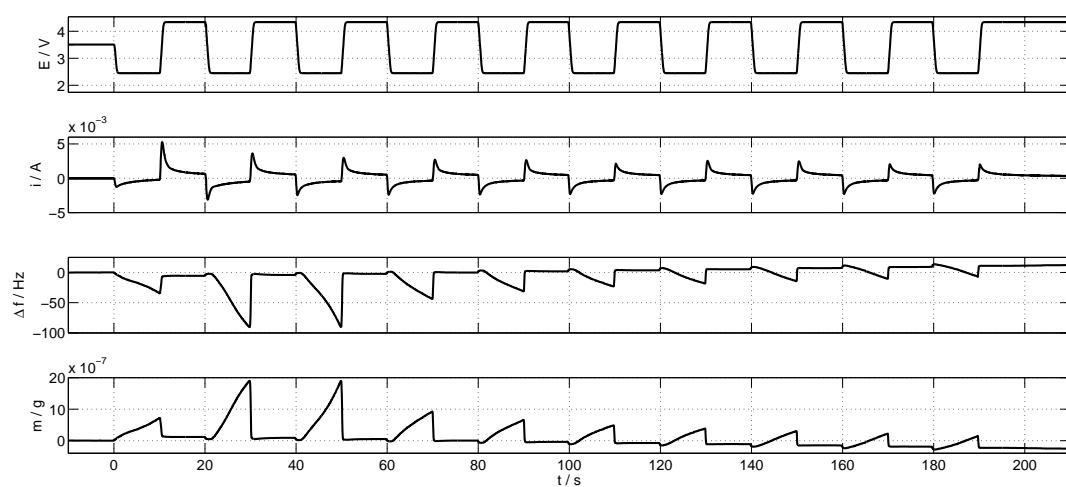
(b) 10 s anodic polarization

Fig. 10 E, i, Δf and m as a function of time during potential cycling between 2.4 V (pulse of 10 s) and 4.3 V (pulse of 10 or 60 s) of O_2 and 0.1 M of Li^+ with TTF on gold.
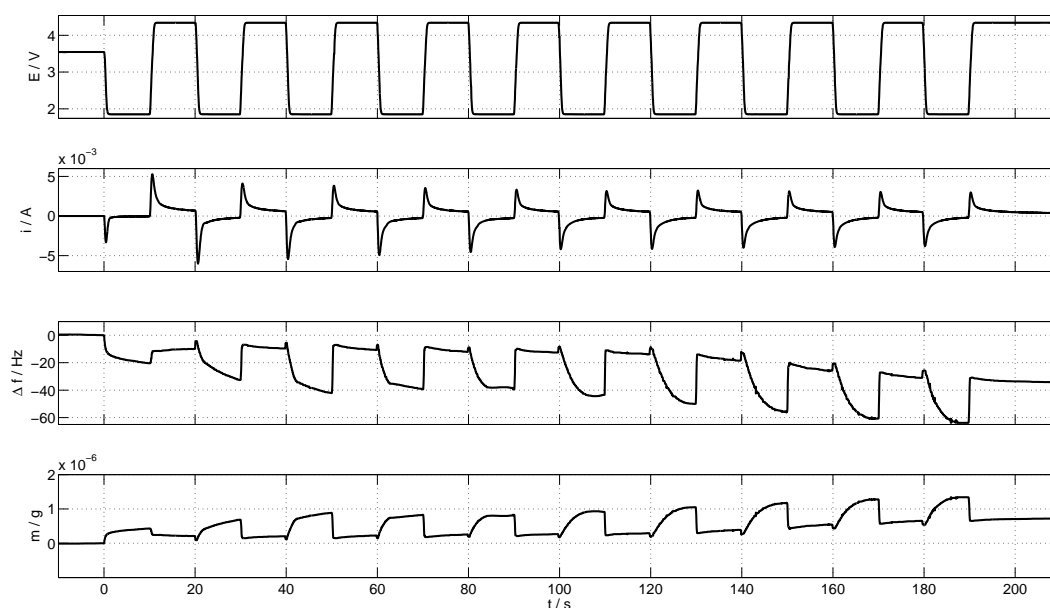
Fig. 11 Potential cycling between 1.8 V and 4.3 V of O_2 and 0.1 M of Li^+ with TTF on gold.

11 C. O. Laoire, S. Mukerjee, K. M. Abraham, E. J. Plichta and M. A. Hendrickson, *J. Phys. Chem. C*, 2009, **113**, 20127–20134.

12 Z. Peng, S. A. Freunberger, L. J. Hardwick, Y. Chen, V. Giordani, F. Bardé, P. Novák, D. Graham, J.-M. Tarascon and P. G. Bruce, *Angew. Chem. Int. Ed.*, 2011, **50**, 6351–6355.

13 F. Bardé, Y. Chen, L. Johnson, S. Schaltin, J. Fransaer and P. G. Bruce, *J. Phys. Chem. C*, 2014, **118**, 18892–18898.

14 K. U. Schwenke, S. Meini, X. Wu, H. A. Gasteiger, Gasteiger and M. Piana, *Phys. Chem. Chem. Phys.*, 2013, **15**, 11830–11839.

15 K. Takechi, S. Higashi, F. Mizuno, H. Nishikoori, H. Iba and T. Shiga, *ECS Electrochem. Lett.*, 2012, **1**, A27–A29.

16 J. T. Frith, A. E. Russell, N. Garcia-Araez and J. R. Owen, *Electrochem. Commun.*, 2014, **46**, 33–35.

17 D. G. Kwabi, T. P. Batcho, C. V. Amanchukwu, N. Ortiz-Vitoriano, P. Hammond, C. V. Thompson and Y. Shao-Horn, *J. Phys. Chem. Lett.*, 2014, **5**, 2850–2856.

18 R. Younesi, P. Norby and T. Vegge, *ECS Electrochem. Lett.*, 2014, **3**, A15–A18.

19 D. Sharon, M. Afri, M. Noked, A. Garsuch, A. A. Frimer and D. Aurbach, *J. Phys. Chem. Lett.*, 2013, **4**, 3115–3119.

20 C. Laoire, S. Mukerjee, K. Abraham, E. Plichta and M. Hendrickson, *J. Phys. Chem. C*, 2010, **114**, 9178–9186.

21 M. J. Trahan, S. Mukerjee, E. J. Plichta, M. A. Hendrickson and K. M. Abraham, *J. Electrochem. Soc.*, 2013, **160**, A259–A267.

22 C. Li, O. Fontaine, S. A. Freunberger, L. Johnson, S. Grugeon, S. Laruelle, P. G. Bruce and M. Armand, *J. Phys. Chem. C*, 2014, **118**, 3393–3401.

23 E. J. Calvo and N. Mozhzhukhina, *Electrochem. Commun.*, 2013, **31**, 56–58.

24 S. E. Herrera, A. Y. Tesio, R. Clarenc and E. J. Calvo, *Phys. Chem. Chem. Phys.*, 2014, **16**, 9925–9929.

25 W. Torres, N. Mozhzhukhina, A. Y. Tesio and E. J. Calvo, *J. Electrochem. Soc.*, 2014, **161**, A2204–A2209.

26 X. Jie and K. Uosaki, *J. Electroanal. Chem.*, 2014, **716**, 49–52.

27 Y. Chen, S. A. Freunberger, Z. Peng, O. Fontaine and P. G. Bruce, *Nat. Chem.*, 2013, **5**, 489–494.

28 M. M. O. Thotiyl, S. A. Freunberger, Z. Peng and P. G. Bruce, *J. Am. Chem. Soc.*, 2013, **135**, 494–500.

29 Z. Peng, S. A. Freunberger, Y. Chen and P. G. Bruce, *Science*, 2012, **337**, 563–566.

30 Y. C. Lu, E. J. Crumlin, G. M. Veith, J. R. Harding, E. Mutora, L. Bagetto, N. J. Dudney, Z. Liu and Y. Shao-Horn, *Sci. Rep.*, 2012, **2**, 715.

31 Y. C. Lu, E. J. Crumlin, T. J. Carney, L. Bagetto, G. M. Veith, N. J. Dudney, Z. Liu and Y. Shao-Horn, *J. Phys. Chem. C*, 2013, **117**, 25948–25954.

32 C. Gabrielli, M. Keddam and R. Torresi, *J. Electrochem. Soc.*, 1991, **138**, 2657–2660.

33 G. Vatankhah, J. Lessard, G. Jerkiewicz, A. Zolfaghari and B. E. Conway, *Electrochim. Acta*, 2003, **48**, 1613–1622.

34 L. Johnson, C. Li, Z. Liu, Y. Chen, S. A. Freunberger, P. C. Ashok, B. B. Praveen, K. Dholakia, J.-M. Tarascon and P. G. Bruce, *Nat. Chem.*, 2014, **6**, 1091–1099.

35 C. Xia, M. Waletzko, L. Chen, K. Peppler, P. J. Klar and J. Janek, *ACS Appl. Mater. Interfaces*, 2014, **6**, 12083–12092.

36 B. D. Adams, C. Radtke, R. Black, M. L. Trudeau, K. Zaghib and L. F. Nazar, *Energy Environ. Sci.*, 2013, **6**, 1772–1778.

37 V. Viswanathan, K. S. Thygesen, J. S. Hummelshøj, J. K. Nørskov, G. Girishkumar, B. D. McCloskey and A. C. Luntz, *J. Chem. Phys.*, 2011, **135**, 214704–214710.